AIAA JOURNAL
Vol. 43, No. 11, November 2005

Kinetic Model Solution for Microscale Gas Flows

Chan H. Chung*
Daegu University, Gyungbuk 712-714, Republic of Korea

A kinetic theory analysis is made of low-speed gas flows around microscale flat plates. The Boltzmann equation simplified by a collision model is solved by means of a finite difference approximation together with the discrete ordinate method. The advantage of the present method is that it does not suffer from statistical noise, which is common in particle-based methods. Calculations are made for flows around a flat plate with zero thickness and a 5% flat plate. Results for the 5% flat plate at a freestream Mach number 0.5 showed good agreement with those from the direct simulation Monte Carlo method. It is shown that strong rarefaction effects exist around the leading and trailing edges. Results from the present method at a freestream Mach number 0.087 also showed similar nonequilibrium effects. Comparison of results with those from the information preservation method and numerical solutions of the Navier–Stokes equations showed some differences in details near the leading and trailing edges.

Nomenclature

A_c	=	collision frequency
d	=	characteristic length of the flowfield
F	=	Maxwell–Boltzmann distribution
f	=	distribution function
g, h	=	reduced distribution functions
Kn	=	Knudsen number
L	=	length of flat plate
l	=	normal distance from plate surface
R	=	gas constant
t	=	thickness of flat plate
U_∞	=	free stream velocity
$\boldsymbol{V}_x$	=	velocity of molecule in the x direction
$\boldsymbol{V}_y$	=	velocity of molecule in the y direction
$\boldsymbol{V}_z$	=	velocity of molecule in the z direction
λ	=	mean free path

I. Introduction

SIMULATION of the flow of rarefied gases around microscale structures such as microelectromechanical systems and micro air vehicles is gaining importance due to the emerging miniaturization technologies. Whereas the fast-growing microscale fabrication technologies result in a wide variety of practical microscale devices, very little numerical work has been performed to analyze the gas flows in and around practical microscale structures.

In microscale structures, the Knudsen number of the flowfield, the ratio of the mean free path to the characteristic dimension of the flowfield, is usually not negligibly small even at atmospheric operating conditions. Hence, conventional computational fluid dynamics methods, which are based on continuum assumptions, may not be appropriate, and a method based on kinetic gas theory is required to describe the flows accurately.

Of the various methods available for the analysis of microscale flows, the direct simulation Monte Carlo (DSMC) method[1] has been used by many researchers.[2–8] The DSMC method has been known to be a robust and accurate method because it is based on kinetic gas theory and does not rely on the continuum assumption that is not valid for high Knudsen number gas flows. Even though the DSMC method has been successfully applied for the analysis of various kinds of rarefied gas flows, simulation of low-speed microscale flows using the DSMC method suffers from several difficulties, including large statistical scatter that has not been encountered in the high-speed gas flow simulations. To get a meaningful result by reducing the large statistical noise, the DSMC method requires a huge amount of computational effort due the number of time steps to reach the steady-state flow condition and the large sample size.[5] These computational demands can render the standard DSMC method impractical given current computing power limitations.

An alternate approach is the information preservation (IP) method developed by Fan and Shen.[9] The IP method preserves macroscopic information while the flowfield is simulated by the DSMC method. The method has been applied to various kind of low-speed flow problems.[9–13] Even though the IP method has been reported to reduce the sampling size by orders of magnitude, the method still requires a large amount of computing effort.

In the present study, a finite difference method coupled with the discrete-ordinate method[14,15] is employed to analyze low-speed gas flows around microscale flat plates. In the method, Boltzmann equation simplified by a collision model [Bhatnagar–Gross–Krook (BGK) equation][16] is solved by means of a finite difference approximation. The physical space is transformed by a general grid-generation technique. The velocity space is transformed to a polar coordinate, and the concept of the discrete ordinate method is employed to discretize the velocity space. The modified Gauss–Hermite quadrature (see Refs. 17 and 18) and Simpson's rule are used for the integration of the discretized velocity space.

To assess the present method, calculations are made for flows around a flat plate with zero thickness and a 5% flat plate. Results are compared with those from the DSMC method, the IP method, and numerical solution of the Navier–Stokes equations with slip boundary conditions.

II. Finite Difference Method

Governing Equation

We consider the steady-state Boltzmann equation with the BGK model[16] in a two-dimensional Cartesian coordinate system:

$$\boldsymbol{V}_x \frac{\partial f}{\partial x} + \boldsymbol{V}_y \frac{\partial f}{\partial y} = A_c(F - f) \tag{1}$$

where $f(x, y, \boldsymbol{V}_x, \boldsymbol{V}_y, \boldsymbol{V}_z)$ is the distribution function, x and y are Cartesian coordinates of the physical space, and $\boldsymbol{V}_x$, $\boldsymbol{V}_y$, and $\boldsymbol{V}_z$ are the velocity components of the molecules. The equilibrium Maxwell–Boltzmann distribution F is given by

$$F = n(2\pi RT)^{-\frac{3}{2}} \exp[-(V - U)^2/2RT] \tag{2}$$

Received 20 June 2004; presented as Paper 2004-2590 at the AIAA 37th Thermophysics Conference, Portland, OR, 28 June–1 July 2004; revision received 24 June 2005; accepted for publication 27 June 2005.

*Professor, Department of Chemical Engineering, Gyungsan. Member AIAA.

The moments n, U, and T can be obtained by integrating the distribution function over the velocity space:

$$n = \int f \, \mathrm{d}V \tag{3a}$$

$$nU = \int V f \, \mathrm{d}V \tag{3b}$$

$$3nRT = \int (V - U)^2 f \, \mathrm{d}V \tag{3c}$$

where n is the particle density and U the macroscopic flow velocity.

The following reduced distribution functions are introduced to reduce the number of independent variables:

$$g(x, y, \boldsymbol{V}_x, \boldsymbol{V}_y) = \int_{-\infty}^{+\infty} f(x, y, \boldsymbol{V}_x, \boldsymbol{V}_y, \boldsymbol{V}_z) \, \mathrm{d}\boldsymbol{V}_z \tag{4a}$$

$$h(x, y, \boldsymbol{V}_x, \boldsymbol{V}_y) = \int_{-\infty}^{+\infty} \boldsymbol{V}_z^2 f(x, y, \boldsymbol{V}_x, \boldsymbol{V}_y, \boldsymbol{V}_z) \, \mathrm{d}\boldsymbol{V}_z \tag{4b}$$

These kinds of reduced distribution functions were first applied by Chu[19] and have been employed by many investigators. The corresponding equations for the reduced distribution functions are obtained by integrating out the $\boldsymbol{V}_z$ dependence with the weighting functions 1 and $\boldsymbol{V}_x^2$, respectively,

$$\boldsymbol{V}_x \frac{\partial g}{\partial x} + \boldsymbol{V}_y \frac{\partial g}{\partial y} = A_c(G - g) \tag{5a}$$

$$\boldsymbol{V}_x \frac{\partial h}{\partial x} + \boldsymbol{V}_y \frac{\partial h}{\partial y} = A_c(H - h) \tag{5b}$$

$$G(x, y, \boldsymbol{V}_x, \boldsymbol{V}_y) = \int_{-\infty}^{+\infty} F \, \mathrm{d}\boldsymbol{V}_z \tag{5c}$$

$$H(x, y, \boldsymbol{V}_x, \boldsymbol{V}_y) = \int_{-\infty}^{+\infty} \boldsymbol{V}_z^2 F \, \mathrm{d}\boldsymbol{V}_z \tag{5d}$$

When the characteristic length of a flowfield d and the most probable speed V_0 defined as

$$V_0 = \sqrt{2RT_0} \tag{6}$$

are used, the following dimensionless variables are introduced:

$$\hat{x} = x/d, \qquad \hat{y} = y/d, \qquad \hat{n} = n/n_0, \qquad \hat{V}_i = V_i/V_0$$

$$\hat{U}_i = U_i/V_0, \qquad \hat{T}_i = T_i/T_0, \qquad \hat{A}_c = \hat{A}_c \, d/V_0$$

$$\hat{g} = gV_0^2/n_0, \qquad \hat{h} = h/n_0, \qquad \hat{G} = GV_0^2/n_0$$

$$\hat{H} = H/n_0, \qquad \hat{\tau} = \tau/\left(1/2mn_0U_\infty^2\right) \tag{7}$$

where the subscript 0 refers to a reference condition.

By the introduction of a polar coordinate system, which is defined as

$$\hat{V}_x = V \sin\phi, \qquad \hat{V}_y = V \cos\phi, \qquad \phi = \tan^{-1}(\hat{V}_x/\hat{V}_y) \tag{8}$$

and application of general transform rules, the governing equations in the new coordinate system (ξ, η) are written as[20]

$$B \frac{\partial \hat{g}}{\partial \eta} + C \frac{\partial \hat{g}}{\partial \xi} = \hat{A}_c(\hat{G} - \hat{g}) \tag{9a}$$

$$B \frac{\partial \hat{h}}{\partial \eta} + C \frac{\partial \hat{h}}{\partial \xi} = \hat{A}_c(\hat{H} - \hat{h}) \tag{9b}$$

$$B = \frac{(\hat{x}_\xi \cos\phi - \hat{y}_\xi \sin\phi)V}{J_t} \tag{9c}$$

$$C = \frac{(\hat{y}_\eta \sin\phi - \hat{x}_\eta \cos\phi)V}{J_t} \tag{9d}$$

Here, J_t is the Jacobian of the transformation.

Discrete Ordinate Method

To remove the velocity–space dependency from the reduced distribution functions, the discrete ordinate method[17,18] is employed. This method, which consists of replacing the integration over velocity space of the distribution functions by appropriate integration formulas, requires the values of the distribution functions only at certain discrete speeds and velocity angles. When discrete distribution functions $\hat{g}_{\delta\sigma}(\xi, \eta, V_\delta, \phi_\sigma)$ and $\hat{h}_{\delta\sigma}(\xi, \eta, V_\delta, \phi_\sigma)$ are employed for the discrete speed V_δ and velocity angle ϕ_σ, the macroscopic moments given by integrals over the molecular velocity space can be substituted by the following quadratures:

$$\hat{n} = \sum_\delta \sum_\sigma P_\delta P_\sigma \hat{g}_{\delta\sigma} \tag{10a}$$

$$\hat{n}\hat{U}_x = \sum_\delta \sum_\sigma P_\delta P_\sigma V_\delta \sin\phi_\sigma \hat{g}_{\delta\sigma} \tag{10b}$$

$$\hat{n}\hat{U}_y = \sum_\delta \sum_\sigma P_\delta P_\sigma V_\delta \cos\phi_\sigma \hat{g}_{\delta\sigma} \tag{10c}$$

$$\frac{3\hat{n}\hat{T}}{2} = \sum_\delta \sum_\sigma P_\delta P_\sigma \left(\hat{h}_{\delta\sigma} + V_\delta^2 \hat{g}_{\delta\sigma}\right) - \hat{n}\left(\hat{U}_x^2 + \hat{U}_y^2\right) \tag{10d}$$

where P_δ and P_σ are weighting factors of the quadratures for the discrete speed V_δ and velocity angle ϕ_σ, respectively. Thus, instead of solving the equations for a function of space and molecular velocity, the equations are transformed to partial differential equations, which are continuous in space but are point functions in molecular speed V_δ and velocity angle ϕ_σ as follows:

$$B_{\delta\sigma} \frac{\partial \hat{g}_{\delta\sigma}}{\partial \eta} + C_{\delta\sigma} \frac{\partial \hat{g}_{\delta\sigma}}{\partial \xi} = \hat{A}_c(\hat{G}_{\delta\sigma} - \hat{g}_{\delta\sigma}) \tag{11a}$$

$$B_{\delta\sigma} \frac{\partial \hat{h}_{\delta\sigma}}{\partial \eta} + C_{\delta\sigma} \frac{\partial \hat{h}_{\delta\sigma}}{\partial \xi} = \hat{A}_c(\hat{H}_{\delta\sigma} - \hat{h}_{\delta\sigma}) \tag{11b}$$

$$B_{\delta\sigma} = \frac{(\hat{x}_\xi \cos\phi_\sigma - \hat{y}_\xi \sin\phi_\sigma)V_\delta}{J_t} \tag{11c}$$

$$C_{\delta\sigma} = \frac{(\hat{y}_\eta \sin\phi_\sigma - \hat{x}_\eta \cos\phi_\sigma)V_\delta}{J_t} \tag{11d}$$

Collision Frequency

The simplest model for the collision integral is the BGK model,[16] which has been widely used and generally gives reasonable results with much less computational effort. In the BGK model, the collision frequency is given by

$$A_c = \psi(P/\mu) \tag{12}$$

where the quantity P is the pressure and ψ is a numerical parameter. The coefficient of viscosity μ is assumed to have a temperature dependency[21]

$$\mu/\mu_0 = (T/T_0)^\omega \tag{13}$$

where the quantity ω is the viscosity index. The equilibrium mean free path for the variable hard sphere (VHS) model[22] is employed:

$$\lambda_0 = \frac{16}{5} \frac{F_k \mu_0}{mn_0\sqrt{2\pi RT_0}} \tag{14}$$

where the quantity F_k is given by

$$F_k = \frac{(5 - 2\omega)(7 - 2\omega)}{24} \tag{15}$$

Combining Eqs. (12–15), we obtain

$$\hat{A}_c = \frac{8\psi F_k \hat{n}\hat{T}^{1-\omega}}{5\sqrt{\pi} K n_0} \tag{16}$$

where $K n_0$ is the Knudsen number at the reference condition based on the characteristic length of the flowfield d.

Boundary Conditions

The following boundary conditions are used for the calculation. At inflow and outflow boundaries, the distribution functions are given by an equilibrium distribution with conditions obtained by using characteristic boundary conditions:

$$f_b = n_b(2\pi RT_b)^{-\frac{3}{2}} \exp\left[-(V-U_b)^2 \big/ 2RT_b\right] \tag{17}$$

where the subscript b refers to conditions at the boundaries.

To specify the interaction of the molecules with the surface, diffuse reflection is assumed, that is, molecules that strikes the surface are subsequently emitted with a Maxwell distribution characterized by the velocity of the surface U_w and the surface temperature T_w:

$$f_w = \tilde{\boldsymbol{n}}_w(2\pi RT_w)^{-\frac{3}{2}} \exp\left[-(V-U_w)^2 \big/ 2RT_w\right] \quad \text{for} \quad (V\cdot\tilde{\boldsymbol{n}}) < 0 \tag{18}$$

where the subscript w refers to conditions at the surface and $\tilde{\boldsymbol{n}}$ is the inward normal vector to the surface. The wall number flux $\tilde{\boldsymbol{n}}_w$ is not known a priori and may be determined by applying the condition of no net flux normal to the surface:

$$\int_{(V\cdot\tilde{n})>0} (V\cdot\tilde{\boldsymbol{n}}) f \,\mathrm{d}V = -\int_{(V\cdot\tilde{n})<0} (V\cdot\tilde{\boldsymbol{n}}) f_w \,\mathrm{d}V \tag{19}$$

Numerical Procedure

Equations (11a) and (11b) are solved by means of finite difference approximations in physical space using simple explicit and implicit schemes depending on the characteristics of physical and velocity space. Details of the method can be found elsewhere.[20] The resulting system of nonlinear algebraic equations is solved by means of successive approximations. In the iterative procedure, only the values of $\hat{A}_c$, $\hat{G}_{\delta\sigma}$, and $\hat{H}_{\delta\sigma}$ have to be determined from moments of the preceding iteration, and the values of distribution functions do not need to be stored. Convergence is assumed to have occurred when the relative differences in the x velocities of two successive iteration steps are less than 10^{-5} for all spatial grid points. As a proper quadrature formula for the discrete speed V_δ, the modified Gauss–Hermite half range quadrature for integrals of the form (see Refs. 15 and 20) is used:

$$\int_0^\infty V^j \exp(-V^2) Q(V)\,\mathrm{d}V = \sum_{\delta=1}^{N} P_\delta Q(V_\delta) \tag{20}$$

The exponent j and the order of the quadrature N in Eq. (20) are chosen to be 1 and 16, respectively. Simpson's three-eighth rule with $\Delta\phi = \pi/30$ is used for the discrete velocity angle. The numerical parameter ψ was chosen to be 0.9, which gives best fit to the DSMC results considered in the present study. In case of the hard sphere molecules, the BGK model parameter ψ usually was assumed to be between $\frac{2}{3}$ and 1 from the well-known behavior of the BGK model,[23] which needs further investigation.

III. Results and Discussion

Flow Around a Flat Plate with Zero Thickness

Consider the steady flow of air around a flat plate with zero thickness and a length $L = 20$ μm. The freestream velocity and temperature are 69 m/s and 295 K, respectively. The freestream Mach number is 0.2. The computational domain is a rectangular region enclosed by the lines $x/L = \pm 20$, $y/L = 0$, and $y/L = 20$. The computational domain is divided into $601(x) \times 201(y)$ nonuniform rectangular grids that are clustered to the plate. Figure 1 shows the computational domain for the simulation. The coefficient of viscosity of air at the reference temperature of 295 K was chosen to be

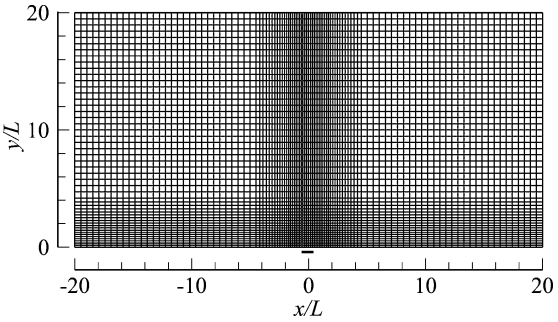

Fig. 1 Computational domain and grid.

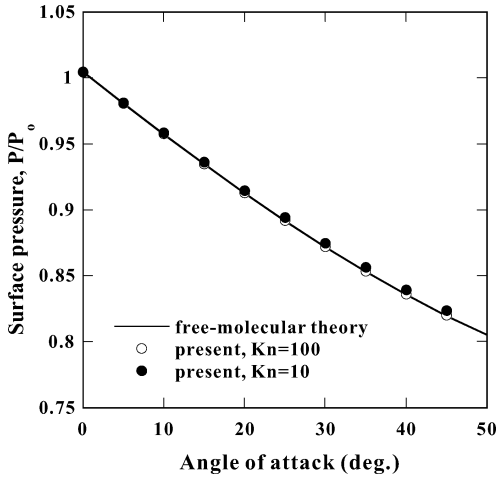

Fig. 2 Comparison of surface pressure distributions at free-molecular flow.

$\mu = 17.64 \times 10^{-6}$ kg/m · s, and the viscosity index ω was chosen to be 0.7.

For the case of free-molecular flow, there are no collisions between molecules, and molecules are moving without collision until reaching the surface of a body. Thus, at any point in the physical space, the velocity space can be divided into two regions, one for molecules coming from the freestream and the other for molecules emitted from the surface. Because exact values of the distribution function can be obtained for each region, theoretical values of moments for free-molecular flow conditions maybe obtained by integrating the distribution function. The free-molecular solution may serve as a good standard for checking the accuracy of a finite difference approximation. In case of the flow around a flat plate with zero thickness, macroscopic moments along the plate surface may be calculated by the following equations:

$$n_w = \exp\left(-U_{\infty,y}^2\right) - \sqrt{\pi} U_{\infty,y}[1 - \mathrm{erf}(U_{\infty,y})] \tag{21}$$

$$n = \tfrac{1}{2} n_w + \tfrac{1}{2}[1 - \mathrm{erf}(U_{\infty,y})] \tag{22}$$

$$nU_{w,x} = \tfrac{1}{2} U_{\infty,x}[1 - \mathrm{erf}(U_{\infty,y})] \tag{23}$$

$$\tfrac{3}{2} nT = \tfrac{3}{4} n_w + \tfrac{1}{2}[1 - \mathrm{erf}(U_{\infty,y})] + \tfrac{1}{4}[1 - \mathrm{erf}(U_{\infty,y})] \times \left(1 + 2U_{\infty,x}^2\right) + \tfrac{1}{2} U_{\infty,y}^2 [1 - \mathrm{erf}(U_{\infty,y})] + \left(U_{\infty,y} \big/ 2\sqrt{\pi}\right) \times \exp\left(-U_{\infty,y}^2\right) - nU_{w,x}^2 \tag{24}$$

$$\tau_w = \left(-2U_{\infty,x} \big/ \sqrt{\pi} U_\infty^2\right)\left\{-\tfrac{1}{2}\exp\left(-U_{\infty,y}^2\right) + \left(\sqrt{\pi}\big/2\right) U_{\infty,y}[1 - \mathrm{erf}(U_{\infty,y})]\right\} \tag{25}$$

Figures 2 and 3 show surface pressure and shear stress, respectively, at $x = L/2$ at the free-molecular condition. In Figs. 2 and 3, the results of the present method at Knudsen numbers of $Kn = 10$

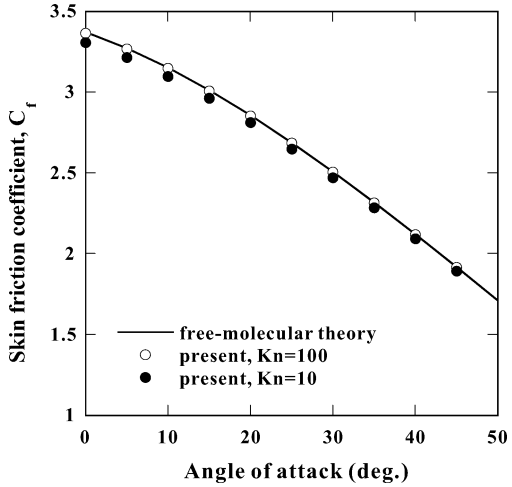

Fig. 3 Comparison of shear stress distributions at free-molecular flow.

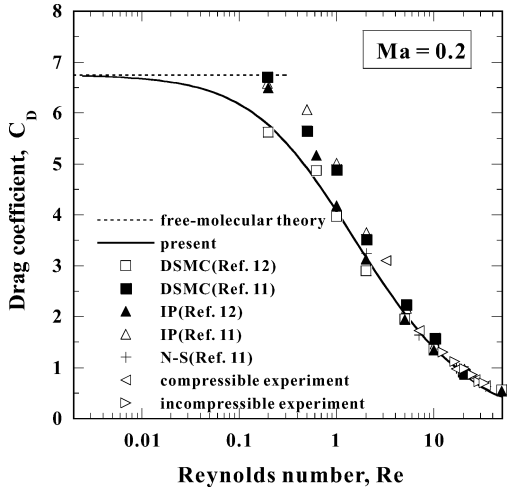

Fig. 4 Drag coefficient of flat plate with zero thickness at low Reynolds numbers.

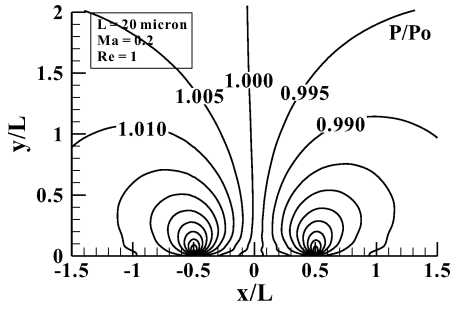

Fig. 5a Pressure contours for $Re = 1$ and $M = 0.2$.

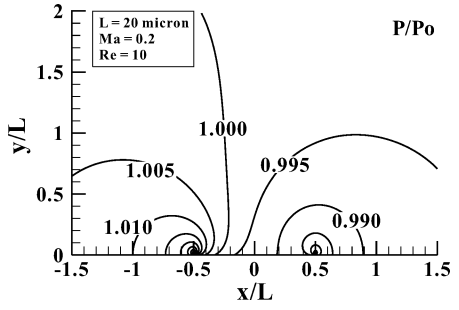

Fig. 5b Pressure contours for $Re = 10$ and $M = 0.2$.

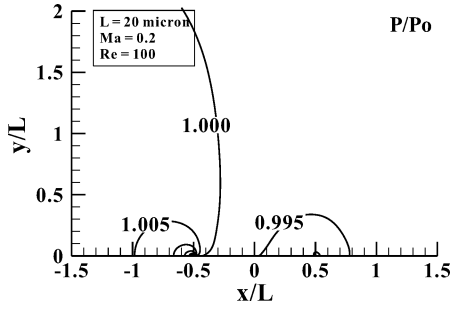

Fig. 5c Pressure contours for $Re = 100$ and $M = 0.2$.

and $Kn = 100$ are compared with the theoretical values at the free-molecular flow condition. The Knudsen number is based on the freestream mean free path and the length of the plate, $Kn = \lambda_\infty / L$. Good agreement is obtained between the calculated results and theoretical values at the free-molecular flow condition.

Figure 4 shows the comparison of the drag coefficient of the plate for both sides at low Reynolds numbers from the DSMC method,[11,12] IP method,[11] and the numerical solutions of the Navier–Stokes (N–S) equations with slip boundary conditions[11] together with experimental data.[24,25] The DSMC and the IP results from Ref. 11 are for a flat plate with a finite length of $L = 20$ μm and those from Ref. 12 are for a plate with a length of $L = 30$ μm, both at the same freestream Mach number 0.2 and temperature 295 K. Note that the scaling law for the normalized drag coefficient of a flat plate at low Reynolds numbers can be expressed by one parameter consisting of only the Reynolds number and the Mach number.[12,26,27] Hence, the drag coefficients for two cases should be similar if both the Reynolds and the Mach numbers are same. Although not shown here, the present method was used to calculate the flowfield around a plate with a length of $L = 30$ μm, and identical results were obtained.

Good agreement is observed among several different methods with experimental data for Reynolds numbers greater than 5. However, the difference between the present and IP methods becomes larger as the Reynolds number decreases. The drag coefficient from the present method is smaller than that from the IP method for the Reynolds numbers smaller than 2 and shows good agreement with the DSMC result from Ref. 12. The drag coefficient from the IP method shows good agreement with the DSMC result from Ref. 11. The drag coefficient from the present method smoothly approaches the free-molecular value around $Re = 0.02(Kn \cong 13)$, whereas that from the IP method approaches the free-molecular value around $Re = 0.2(Kn \cong 1.3)$.

Figure 5 shows the effect of Reynolds number on the pressure contours. It can be seen that as Reynolds number decreases, that is, as the flow becomes more rarefied, the disturbance of the flow caused by the solid object becomes larger. This is because as the flow becomes more rarefied the molecules that collided with the surface can travel more distance without experiencing collision between molecules.

Flow Around a 5% Flat Plate

Consider the steady flow of air around a 5% (thickness-to-length ratio) flat plate with an angle of attack of 10 deg. The length and the thickness of the plate are $L = 20$ μm and $t = 1$ μm, respectively. To investigate the overall characteristics of the flowfield and to compare results from the present method with those from the DSMC method, a relatively high-speed flow of $M = 0.5$ has been chosen. The freestream temperature is 295 K and the Reynolds number is 23. The computational domain is a rectangular region enclosed by the lines $x/L = \pm 20$ and $y/L = \pm 20$. The computational domain is divided into $2 \times 421(x) \times 141(y)$ (upper and lower sides) $+ 2 \times 141(x) \times 21(y)$ (left- and right-hand sides) nonuniform rectangular grids that are clustered to the plate.

Because of limitations in computational resources, the computational domain for the DSMC calculation has been chosen to

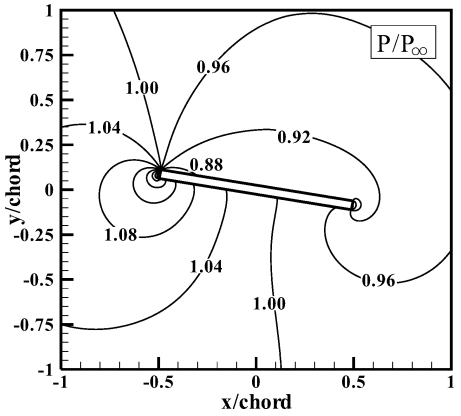

Fig. 6a Pressure contours from present method at $M = 0.5$ and $Re = 23$.

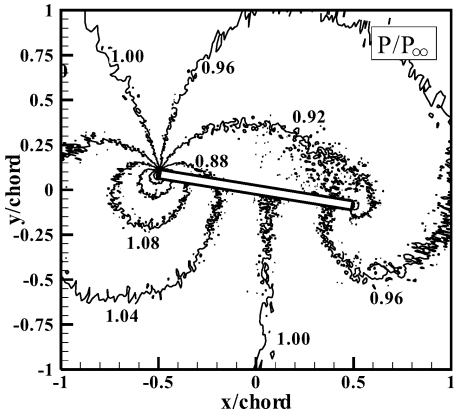

Fig. 6b Pressure contours from DSMC method at $M = 0.5$ and $Re = 23$.

be a rectangular region enclosed by the lines $x/L = \pm 1.7$ and $y/L = \pm 1.025$. The macroscopic flow variables obtained by the present method have been used as boundary conditions for the DSMC calculation. About 32,000 nonuniform rectangular cells that are clustered to the plate is employed with about 1,250,000 particles and 13,000 sampling time steps (average sampling size of 0.5 million per cell) after 10,000 time steps of development. The DSMC code used in the present study is based on the same principles as described by Bird[1] together with the VHS model[22] as a molecular model and the no time counter (NTC) method[28] as a collision sampling technique. The code has been applied to various low-density flows of gas mixtures in arbitrary shaped flow domains.[29,30] Details of the code may be found in Ref. 29. Calculated pressure contours are compared in Fig. 6. It can be seen that the results from the present and the DSMC methods show good agreement. Figure 7 shows skin friction on the upper and lower surfaces given by

$$C_f = \tau_w / 0.5 \rho_\infty U_\infty \tag{26}$$

The shear stress τ_w is calculated by sampling (DSMC method) or integrating (present method) the parallel momentum transfer rate from the gas molecules to the surface. It can be seen that the magnitude of skin friction increases near the leading and trailing edges.

Figure 8 shows pressure coefficients on and near the upper surface, which is given by

$$C_P = \frac{P - P_\infty}{0.5 \rho_\infty U_\infty} \tag{27}$$

On the surface, the pressure is calculated by sampling (DSMC method) or integrating (present method) the normal momentum transfer rate from the gas molecules to the surface. Near the surface, the pressure is calculated by using the ideal gas law. In Fig. 8, the quantity t is the thickness of the plate and l is the normal distance from the surface. It is interesting to see that the pressure coefficients

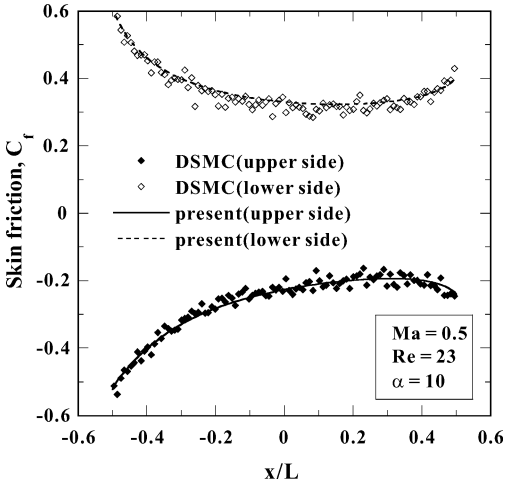

Fig. 7 Shear stress distributions at $M = 0.5$ and $Re = 23$.

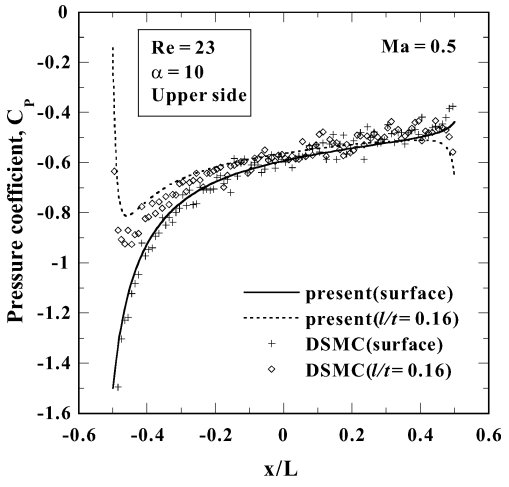

Fig. 8 Pressure coefficients on and near the upper surface at $M = 0.5$ and $Re = 23$.

on and near the surface show opposite behavior. The pressure coefficient along the line of $l/t = 0.16$ (that is, 0.16 μm away from the surface) shows maximum at the leading edge, decreases abruptly, shows local minimum, and increases. Around the trailing edge, the pressure coefficient along the line of $l/t = 0.16$ decreases abruptly. However, the pressure coefficient on the surface shows a minimum at the leading edge, increases rapidly near the leading edge, and increases slowly toward the trailing edge.

Figure 9 shows pressure coefficients on and near the lower surface. The pressure coefficient along the line of $l/t = -0.16$ decreases continuously from the leading edge to the trailing edge. However, the pressure coefficient on the surface slightly increases near the trailing edge. Comparison of results from the present method with those from the DSMC methods around the leading and trailing edges shows that the present method can accurately predict the strong rarefaction effects in these strong nonequilibrium regions.

The next problem considered is a low-speed flow around a 5% flat pate. The freestream Mach number is 0.087 and the Reynolds number is 4. Calculated pressure contours are compared in Fig. 10 with those from the IP method[11] and the continuum approach.[11] It can be seen that the results from the three different methods show relatively good agreement except for the small differences in the magnitude and shape of the contours. For example, the contours from the present and the continuum methods have circular shapes, whereas those from the IP method are closer to ellipses.

Figure 11 shows a comparison of skin friction on the upper and lower surfaces from the three different methods. It can be seen that calculated skin frictions from the present and the IP methods show

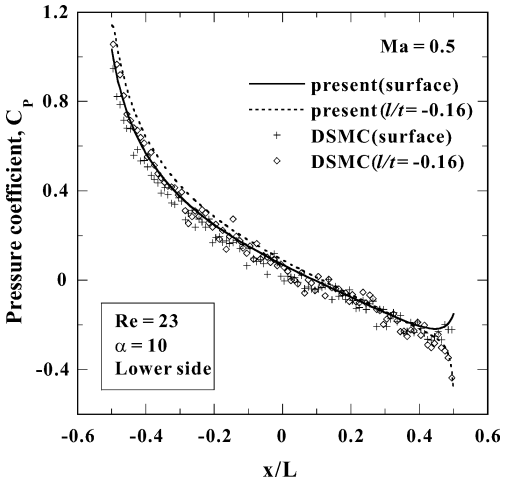

Fig. 9 Pressure coefficients on and near the lower surface at $M = 0.5$ and $Re = 23$.

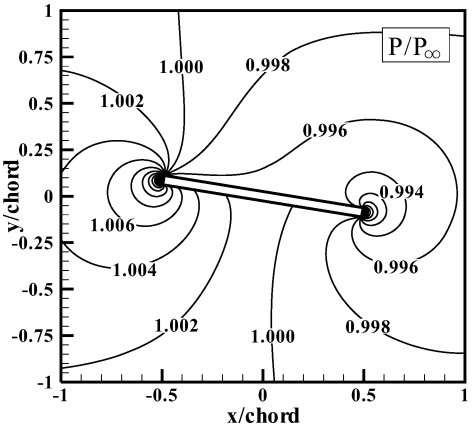

Fig. 10a Pressure contours at $M = 0.087$ and $Re = 4$, present method.

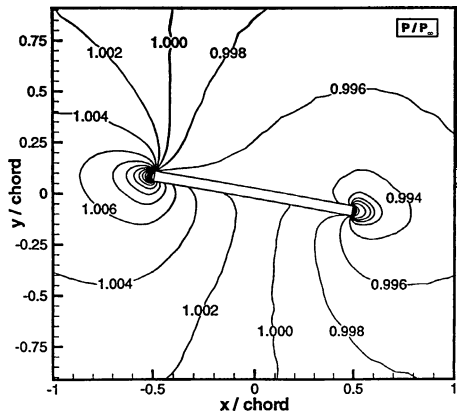

Fig. 10b Pressure contours at $M = 0.087$ and $Re = 4$, IP method (Ref. 11).

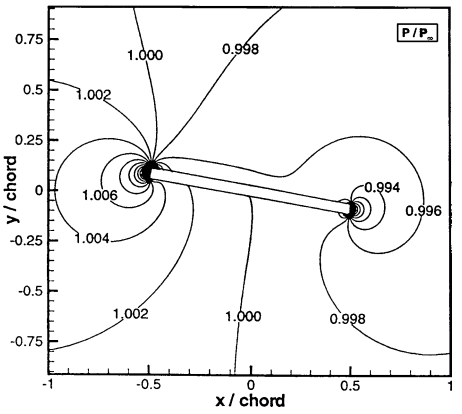

Fig. 10c Pressure contours at $M = 0.087$ and $Re = 4$, continuum method (Ref. 11).

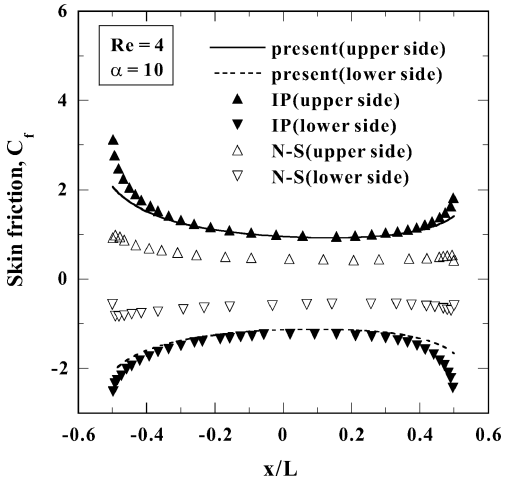

Fig. 11 Skin-friction distributions on surface at $Re = 4$.

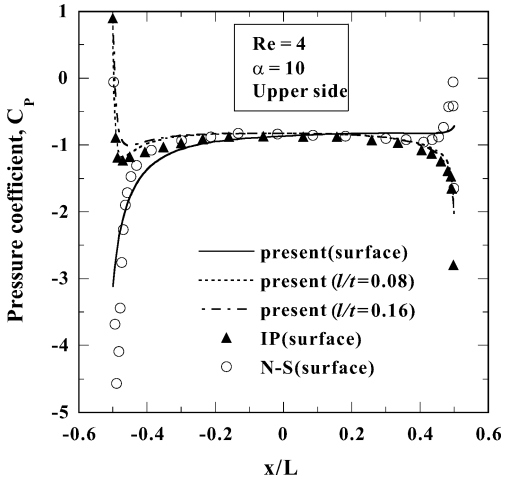

Fig. 12 Pressure coefficients on and near upper surface at $Re = 4$.

good agreement except for some differences near the leading and trailing edges. The magnitude of skin friction from the continuum approach[11] is smaller than that from the molecular approaches.

The calculated pressure coefficients on and near the upper surface are compared in Fig. 12 with those from the IP method[11] and the continuum approach.[11] The calculated pressure coefficients from the three different methods show good agreement except for some differences near the leading and trailing edges, where strong rarefaction effects exist. To investigate the differences in the pressure coefficients near the leading and trailing edges, the pressure coefficients on and at a short distance away from the upper surface are compared. The pressure coefficients from the present method show similar behavior observed in the earlier case of $M = 0.5$. That is, the pressure coefficient near the surface shows maximum at the leading edge, decreases abruptly, shows local minimum, and increases. Around the trailing edge, the pressure coefficient decreases abruptly. The pressure coefficient on the surface shows a minimum at the leading edge, increases rapidly near the leading edge, and increases slowly toward the trailing edge. In the IP method, the information of the particles is set as the wall condition if it is a diffuse reflection and equations based on free-molecular theory are employed for the calculation of surface quantities.[11] It can be seen

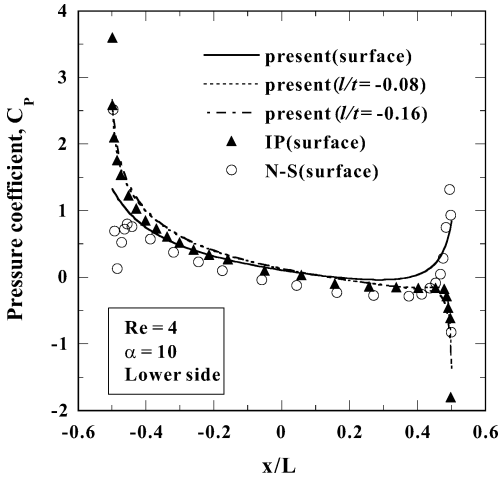

Fig. 13 Pressure coefficients on and near lower surface at $Re = 4$.

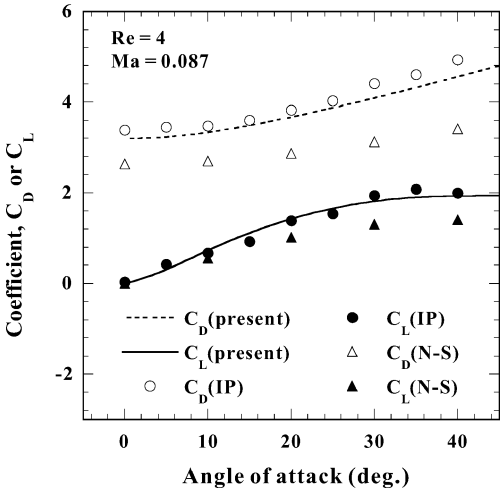

Fig. 14 Characteristics of 5% flat plate at $Re = 4$.

that the surface pressure coefficient from the IP method shows similar behavior to those along the lines of $l/t = 0.08$ and 0.16 from the present method, which may show that the models used in the IP method can not capture all necessary physics in the strong nonequilibrium regions. It is interesting that the pressure coefficient from the continuum method[11] shows behavior similar to those from the present method, although the magnitude is slightly larger.

The calculated pressure coefficients on and near the lower surface are compared in Fig. 13 with those from the IP method[11] and the continuum approach.[11] Again, the calculated pressure coefficients from the three different methods show good agreement except for some differences near the leading and trailing edges, where strong rarefaction effects exist. The surface pressure coefficient from the present method show similar behavior that observed in the case of $M = 0.5$. The surface pressures from the IP method are closer to those along the lines of $l/t = -0.08$ and -0.16 from the present method.

The aerodynamic characteristics of the 5% plate are shown in Fig. 14. It can be seen that the lift from the present and IP methods show good agreement and the drag from the present method is slightly smaller than that from the IP method.[11] The drag and the lift from the continuum approach are much smaller than those from the present and IP methods. The ratio of lift to drag from three methods is shown in Fig. 15. For comparison, the theoretical ratio of lift to drag for free-molecular flow and that from the present method at $Re = 0.015$ are shown together. It can be seen that the ratio of lift to drag from the three methods show relatively good agreement.

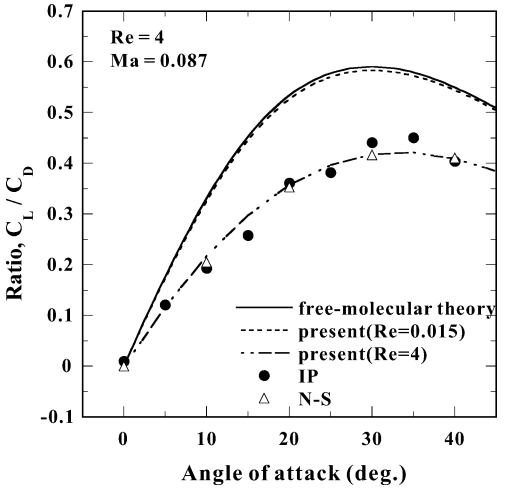

Fig. 15 Comparison of C_L/C_D at $Re = 4$.

IV. Conclusions

A finite difference method coupled with the discrete-ordinate method is employed to analyze low-speed gas flows around microscale flat plates. Calculations are made for flows around a flat plate with zero thickness and a 5% flat plate. Results are compared with those from the DSMC method, the IP method, and numerical solutions of the N–S equations with slip boundary conditions. The calculated results show good agreement, except for some differences in details near the leading and trailing edges. The calculated pressure on and at a short distance away from the surface showed quite different behavior, especially in the region close to the leading edge where rarefaction effects play an important role. The behavior of the surface pressure from the IP method was closer to that of the present method at a short distance away from the surface rather than that on the surface, which may show that the models used in the IP method can not capture all necessary physics in the strong nonequilibrium regions. The advantage of the present method is that it does not suffer from statistical noise that is common in particle-based methods. All of the calculations in the present work are performed in a desktop computer with a Pentium IV 3.2-GHz processor. CPU time required for the present calculations varies from about 15 min (plate with zero thickness at $Re = 0.002$) to about 190 h (5% plate at $Re = 4$ and angle of attack 45 deg) depending on the degree of rarefaction and the flow speed.

References

[1]Bird, G. A., *Molecular Gas Dynamics and the Direct Simulation of Gas Flows*, Clarendon, Oxford, 1994.

[2]Ikegawa, M., and Kobayashi, J., "Development of a Rarefied Flow Simulator Using the Direct-Simulation Monte-Carlo Method," *JSME International Journal, Series 2*, Vol. 33, No. 3, 1990, pp. 463–467.

[3]Piekos, E. S., and Breuer, K. S., "Numerical Modeling of Micromechanical Devices Using the Direct Simulation Monte-Carlo Method," *Transactions of the American Society of Mechanical Engineers*, Vol. 118, Sept. 1996, pp. 464–469.

[4]Mavriplis, C., Ahn, J. C., and Goulard, R., "Heat Transfer and Flowfields in Short Microchannels Using Direct Simulation Monte Carlo," *Journal of Thermophysics and Heat Transfer*, Vol. 11, No. 4, 1997, pp. 489–496.

[5]Oh, C. K., Oran, E. S., and Sinkovits, R. S., "Computations of High-Speed, High Knudsen Number Microchannel Flows," *Journal of Thermophysics and Heat Transfer*, Vol. 11, No. 4, 1997, pp. 497–505.

[6]Nance, P. R., Hash, D. B., and Hassan, H. A., "Role of Boundary Conditions in Monte Carlo Simulation of Microelectromechanical Systems," *Journal of Thermophysics and Heat Transfer*, Vol. 12, No. 3, 1998, pp. 447–449.

[7]Mott, D. R., Oran, E. S., and Kaplan, C. R., "Microfilter Simulations and Scaling Laws," *Journal of Thermophysics and Heat Transfer*, Vol. 15, No. 4, 2001, pp. 478–483.

[8]Fang, Y., Liou, W. W., and Bird, G. A., "Three-Dimensional Simulation of Micro Rayleigh–Benard Convection by DSMC," AIAA Paper 2004-2671, July 2004.

[9]Fan, J., and Shen, C., "Statistical Simulation of Low-Speed Unidirectional Flows in Transition Regime," *Rarefied Gas Dynamics*, Vol. 2, edited by R. Brun, R. Campargue, R. Gatignol, and J. C. Lengrand, Cepadues-Editions, Toulouse, France, 1999, pp. 245–252.

[10]Cai, C., Boyd, I. D., Fan, J., and Candler, G. V., "Direct Simulation Methods for Low-Speed Microchannel Flows," *Journal of Thermophysics and Heat Transfer*, Vol. 14, No. 3, 2000, pp. 368–378.

[11]Sun, Q., Boyd, I. D., and Candler, G. V., "Numerical Simulation of Gas Flow over Micro-Scale Airfoils," *Journal of Thermophysics and Heat Transfer*, Vol. 16, No. 2, 2001, pp. 171–179.

[12]Sun, Q., and Boyd, I. D., "Drag on a Flat Plate in Low Reynolds Number Gas Flows," *AIAA Journal*, Vol. 42, No. 6, 2004, pp. 1066–1072.

[13]Sun, Q., and Boyd, I. D., "Flat-Plate Aerodynamics at Very Low Reynolds," *Journal of Fluid Mechnics*, Vol. 502, 2004, pp. 199–206.

[14]Chung, C. H., De Witt, K. J., Jeng, D. R., and Keith, T. G., Jr., "Numerical Analysis of Rarefied Gas Flow Through Two-Dimensional Nozzles," *Journal of Propulsion and Power*, Vol. 11, No. 1, 1995, pp. 71–78.

[15]Huang, A. B., "The Discrete Ordinate Method for the Linearized Boundary Value Problems in Kinetic Theory of Gases," Rarefied Gas Dynamics and Plasma Lab., Rept. 4, School of Aerospace Engineering, Georgia Inst. of Technology, Atlanta, 1967.

[16]Bhatnagar, P. L., Gross, E. P., and Krook, M., "A Model for Collision Processes in Gases. I. Small Amplitude Processes in Charged and Neutral One-Component Systems," *Physical Review*, Vol. 94, No. 3, 1954, pp. 511–525.

[17]Huang, A. B., and Giddens, D. P., "A New Table for a Modified (Half-Range) Gauss–Hermite Quadrature with an Evaluation of the Integral," *Journal of Mathematics and Physics*, Vol. 47, March 1968, pp. 213–218.

[18]Shizgal, B., "A Gaussian Quadrature Procedure for Use in the Solution of the Boltzmann Equation and Related Problems," *Journal of Computational Physics*, Vol. 41, No. 2, 1981, pp. 309–328.

[19]Chu, C. K., "Kinetic–Theoretic Description of the Formation of a Shock Wave," *Physics of Fluids*, Vol. 8, No. 1, 1965, pp. 12–22.

[20]Chung, C. H., "Numerical Simulation of Rarefied Gas Flow Through Nozzles and over Submerged Bodies," Ph.D. Dissertation, Dept. of Chemical Engineering, Univ. of Toledo, Toledo, OH, June 1990.

[21]Chapman, S., and Cowling, T. G., *The Mathematical Theory of Non-Uniform Gases*, Cambridge Univ. Press, London, 1958, pp. 218–234.

[22]Bird, G. A., "Monte Carlo Simulation in an Engineering Context," *Rarefied Gas Dynamics*, Progress in Astronautics and Aeronautics, edited by Sam S. Fisher, Vol. 74, Pt. 1, AIAA, New York, 1981, pp. 239–255.

[23]Atassi, H., and Shen, S. F., "A Unified Kinetic Theory Approach to External Rarefied Gas Flows. Part 1. Derivation of Hydrodynamic Equations," *Journal of Fluid Mechanics*, Vol. 53, Pt. 3, 1972, pp. 417–431.

[24]Dennis, S. C., and Dunwoody, J., "The Steady Flow of a Viscous Fluid past a Flat Plate," *Journal of Fluid Mechanics*, Vol. 24, No. 3, 1966, pp. 577–595.

[25]Schaaf, S. A., and Sherman, F. S., "Skin Friction in Slip Flow," *Journal of the Aeronautical Sciences*, Vol. 21, No. 2, 1954, pp. 85–89.

[26]Schaaf, S. A., "A Note on the Flat Plate Drag Coefficient," Inst. of Engineering Research, Rept. HE-150-66, Univ. of California, Berkeley, CA, 1950.

[27]Mirels, H., "Estimate of Slip Effect on Compressible Laminar-Boundary-Layer Skin Friction," NACA TN 2609, Jan. 1952.

[28]Bird, G. A., "The Perception of Numerical Methods in Rarefied Gas Dynamics," *Rarefied Gas Dynamics*, Vol. 118, Progress in Astronautics and Aeronautics, edited by E. P. Muntz, D. P. Weaver, and D. H. Campbell, AIAA, Washington, DC, 1989, pp. 211–226.

[29]Chung, C.-H., De Witt, K. J., Stubbs, R. M., and Penko, P. F., "Simulation of Overexpanded Low-Density Nozzle Plume Flow," *AIAA Journal*, Vol. 33, No. 9, 1995, pp. 1646–1650.

[30]Chung, C. H., Kim, S. C., De Witt, K. J., and Nagamatsu, H. T., "Numerical Analysis of Hypersonic Low-Density Scramjet Inlet Flow," *Journal Spacecraft and Rockets*, Vol. 32, No. 1, 1995, pp. 60–66.

C. Kaplan
Associate Editor